Influence of Cloud Characteristics on PPM Optical Communication Rate

Binyu Li, Bo Li, Xueying Zhang, Chaoqun Wang, Lei Zhang, and Shoufeng Tong

***Abstract*—Pulse position modulation (PPM) is a key technology for deep space optical communication (DSOC) system to improve the data transmission rate. To reach optimum rate, the modulation parameters of PPM are required to be analyzed. The rate can be improved by choosing appropriate modulation orders and the initial pulse width. In this paper, the meteorological statistical data of our experimental location are analyzed. Then, the analysis formula of the cloud scattering and atmospheric turbulence influence on PPM communication rate are given. The cloud particles are measured through aircraft detector, simulation analysis is carried out by using the measured data of aircraft detector. Finally, the influence on the communication rate of different cloud physical thickness are analyzed.**

***Index Terms*—Atmospheric channel, pulse broadening, PPM, optical communication rate.**

I. Introduction

COMPARED with the microwave communication, optical communication between ground stations and satellites offers several significant advantages, such as smaller size and mass of system, less power consumption on satellite terminal, more immune to interference, lower probability of interception, larger data rate [1]–[3]. It also has a broad prospect for deep space exploration system to greatly improve the data transmission rate [4]–[8].

Pulse position modulation (PPM) provides an energy-efficient means of using high peak power laser for transmitting signals from deep space to earth-based receiving stations [9]–[11]. In the 2^M-ary PPM modulation scheme, each channel symbol period is divided into 2^M equal non-overlapping time slots, and the information comprised of M bits is sent by pulsing the optical intensity in one of these slots. Each slot is very short ($\sim ns$), but the laser power that the signal slot contained is very high ($\sim$kW). Therefore, the PPM can compensate the huge link loss and suppress the background photons, and now it is the preferred technique for DSOC system. It should be noted that PPM results in a relative low communication rate in comparison with the other modulation methods and it seldom used in high rates demanded FSO systems now, but it can bring a pretty good rate gain to DSOC.

The relationship between PPM parameters and the wireless optical communication performances has been widely studied, especially in the research of its BER performance in turbulence channel. For example, the error performance of PPM channels in turbulent atmosphere with lognormal density distribution and Gamma-Gamma distribution were investigated respectively [12], [13]. Chatzidiamantis studied the error performance with inverse Gaussian distribution [14]. Accurate BER computation for 2^M-ary PPM was proposed by Beaulieu and Hamkins [15], [16]. A deep discussion about PPM communication rate is meaningful in DSOC, and it also required in MIMO-PPM of optical wireless [17], [18]. But the literatures about relationship between PPM parameters and the data transmission rate are limited. The capacity of PPM on Gaussian and Webb Channels was computed, the results showed that the capacity depended on the physical parameters of the APD and the constraints imposed by the orthogonal signaling set [19]. Several properties of the channel capacity that lead to an appropriate selection of modulation format, PPM order, and error-control code rate were described by Moision [20].

However, the laser pulse broadening and delay caused by cloud and atmospheric turbulence also can degrade the communication performance, as shown in Fig. 1. The transmitting signal is in the second slot at the start, but the received signal is broadened and then occupies the next two consecutive slots. This phenomenon will lead to BER increase. One method for solving this problem is to increase the slot width, as a result, it reduces the data rate and heavily decreases the performance of DSOC data transfer. Therefore, the influence of pulse broadening on DSOC system must be taken into consideration. However, little work has been done on this and the literatures mentioned above only discussed the capacity or communication rate under different attenuation distribution models without taking the degradations into account. In this paper, we focus on the influence of cloud on PPM, and the analysis formula is derived. Then, the relationship

Manuscript received September 14, 2021; revised November 12, 2021; accepted November 23, 2021. Date of publication November 30, 2021; date of current version December 22, 2021. This work was supported in part by the Department of Science and Technology of Jilin province under Project 20200201010JC, and in part by the Project of the Science and Technology Department of Jilin Province under Grant 20210204122YY. *(Corresponding author: Shoufeng Tong.)*

Binyu Li is with the Institute of Photoelectric Engineering, Changchun University of Science and Technology, Changchun 130022, China (e-mail: custlby@163.com).

Bo Li is with the Institute of Deep-sea Science and Engineering, Chinese Academy of Sciences, Sanya 572000, China (e-mail: 82609899@qq.com).

Xueying Zhang is with the Jilin Weather Modification Office, Changchun 130022, China (e-mail: zhangxueying14@lzu.edu.cn).

Chaoqun Wang is with the Jilin Center for Meteorological Disaster Prevention Technology, Changchun 130022, China (e-mail: 406860886@qq.com).

Lei Zhang and Shoufeng Tong are with the Institute of Space Photoelectric Technology, Changchun University of Science and Technology, Changchun 130022, China, and also with the Institute of Space Photoelectric Technology, Changchun University of Science and Technology, Changchun 130022, China (e-mail: 1422359488@qq.com; cust0888@163.com).

Digital Object Identifier 10.1109/JPHOT.2021.3131247

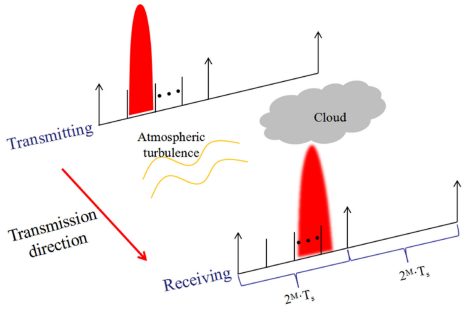

Fig. 1. The illustration of pulse broadening and time delay caused by atmosphere channel.

between pulse broadening and the DSOC communication rate are described. Through aircraft detection test and the detection or prediction of actual atmospheric conditions, we draw a conclusion, the rate can be improved by choosing appropriate modulation orders and the initial pulse widths.

II. Theoretical Analysis

A. Cloud

Scattering optical thickness of cloud with uniform density can be expressed as

$$\tau_d = T/D_d \tag{1}$$

τ_d is the cloud optical thickness of the effective scattering part, T is the cloud physical thickness, and D_d is the average multipath scattering length in the effective scattering cloud,

$$D_d = D/(1 - \langle\cos\theta\rangle) \tag{2}$$

D is the average free path length between continuous scattering; $<\cos\theta>$ is the average cosine of included angle which is between incident light and scattered light. In isotropic scattering medium, D is the reciprocal of extinction coefficient, so it can be obtained [21],

$$D = (N\pi r^2 Q_{ext})^{-1} \tag{3}$$

Where Q_{ext} is the extinction efficiency factor and N is the scattering number with unit volume.

$$\tau_d = T \cdot N\pi r^2 Q_{ext}(1 - \langle\cos\theta\rangle) \tag{4}$$

LWC is the liquid water content of the cloud at the observation, ρ is the density of water, r_0 is the average radius of cloud particle at the observation. Q_{ext} and $<\cos\theta>$ are the function of the water droplet radius. The average value is taken [21],

$$LWC = (4\pi/3)Nr_0^3\rho = 4/3\rho r_0 \cdot N\pi r_0^2 \tag{5}$$

$$r(t) = r_0[1 - (t/T)]^{\frac{1}{3}} \tag{6}$$

Integrate over τ_d,

$$\begin{aligned}\tau_d &= \int_0^T N\pi r^2 Q_{ext}(1 - \langle\cos\theta\rangle)dt \\ &= \int_0^T \frac{0.75LWC}{\rho r_0}[1 - (t/T)]^{\frac{2}{3}} Q_{ext}(1 - \langle\cos\theta\rangle)dt \\ &= \frac{0.45LWC \cdot Q_{ext}\left(1 - \langle\cos\theta\rangle\right)T}{\rho r_0}\end{aligned} \tag{7}$$

E. A. Bucher group established experimental relation of the time interval $\triangle t$ and scattering optical thickness through experimental statistical data [22],

$$\Delta t = \frac{0.74}{c}\tau_d^{0.82} \tag{8}$$

Eq. (7) is combined with Eq. (8),

$$\Delta t = \frac{0.74}{c}\left(\frac{0.45LWC \cdot Q_{ext}\left(1 - \langle\cos\theta\rangle\right)T}{\rho r_0}\right)^{0.82} \tag{9}$$

The maximum communication rate R_c can be achieved after pulse broadening under PPM modulation [23],

$$R_c = \frac{M}{(t_0 + \Delta t) \cdot 2^{M+1}} \tag{10}$$

Jilin Province is located in the middle latitudes of the northern hemisphere and situated in the hinterland of the Songliao Plain in northeast China. The central geographic coordinate of jilin Province is N43°55', E125°18'. The average precipitation of summer is 522-615mm, more than 60% of the precipitation of the year is concentrated in summer. The weather is sunny and dry in autumn and winter, and the occurrence probability of cumulus and stratus are very low [24]. According to the cloud cover statistical report provided by China Meteorological Administration, cirrus occurs less than 10% in most areas of China, but the occurrence probability in some areas of Jilin Province is up to 60%.

Cirrus is composed of small ice crystals in high-altitude, and the distribution of particles is sparse, and the cloud thickness is thin. The horizontal range of cirrus can reach hundreds to thousands of kilometers, and the life span can reach several hours to several days. Although cirrus has less attenuation (1∼2dB) on optical signal comparing with other clouds [1], in view of the high occurrence probability of cirrus in Jilin Province, the influence of cirrus on space optical communication must be considered when analyzing the slant link of space optical communication.

The extinction efficiency for a sphere of radius r can be approximated as follows [25],

$$\begin{aligned}Q'_{ext}(\beta,\rho) &= 2 - 4\exp(-\rho\tan\beta)\left[\frac{\cos\beta}{\rho}\sin(\rho-\beta)\right. \\ &\left. + \left(\frac{\cos\beta}{\rho}\right)^2\cos(\rho-2\beta)\right] + 4\left(\frac{\cos\beta}{\rho}\right)^2\cos 2\beta\end{aligned} \tag{11}$$

Where $\rho = 2\chi|m_r - 1|$ is the phase delay that the ray passes through particle. The phase shift of the transmitted ray is given though $\beta = \tan^{-1}(m_i/(m_r - 1))$. The extinction efficiency of non-spherical ice crystal can be expressed like this,

$$\begin{aligned}&Q''_{ext}(\rho_e,\beta,\alpha) \\ &= 2\left[1 - \exp\left(-\frac{2}{3}\rho_e\tan\beta\right)\cos\left(\frac{2}{3}\rho_e + \alpha\right)\right]\end{aligned} \tag{12}$$

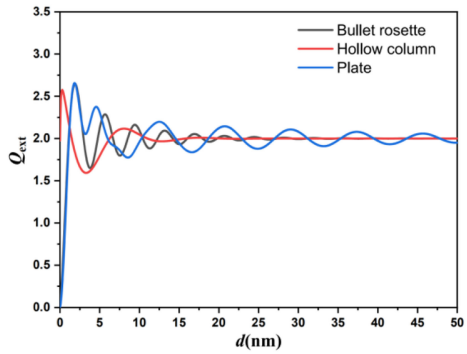

Fig. 2. Extinction efficiency factors of different particle forms in cirrus clouds.

where $\rho_e = 2\pi d_e|m_r - 1|/\lambda$ is the effective phase delay. To account for the complex ray behavior inside the ice crystal, Eqs. (11) and (12) are combined to given the extinction efficiency of effective phase delay ρ_e,

$$Q_{ext}(D, m_r, m_i) = (1-\xi)\, Q'_{ext}(\beta_1, \eta_1\rho_e) + \xi Q''_{ext}(\eta_2\rho_e, \beta_2, \alpha) \quad (13)$$

Ice crystal particles in cirrus clouds have many typical forms. The mathematical model of particles scattering characteristics can be obtained through calculating the extinction efficiency factor of each form and the proportion in cirrus cloud. When the maximum size of ice crystal particles in cirrus clouds is small, the midlatitude cirrus clouds consist of 50% bullet rosettes, 25% hollow columns and 25% plates [26].

Then, according to the scattering database of ice crystal particles given in reference [27], the extinction efficiency factor of main ice crystal particles in cirrus cloud can be obtained and shown in Fig. 2 .

B. Turbulence

Atmospheric turbulence also can result in pulse broadening effect, the broadening time caused by atmospheric turbulence can be expressed as [28]

$$T_1 = \sqrt{T_0^2 + 8\alpha} \quad (14)$$

where T_0 is the initial pulse width, α is the turbulence parameter which represents the phase fluctuations of the pulse, and it is defined by

$$\alpha = \frac{0.391\left(1 + 0.171\delta^2 - 0.287\delta^{5/3}\right)\mu_1 \sec\zeta}{c^2} \quad (15)$$

$\delta = l_0(h)/L_0(h)$, δ is the ratio of inner scale to outer scale, ζ is the zenith angle, and μ_1 is the parameter related to altitude that can be evaluated numerically,

$$\mu_1 = \int_{h_0}^{h_f} C_n^2(h)\left[\kappa_0(h)\right]^{-5/3} \mathrm{d}h \quad (16)$$

where $\kappa_0(\mathrm{h}) = 1/L_0(h)$, $C_n^2(h)$ is the refractive-index structure constant which is adopted to H-V21 model [1],

$$C_n^2(h) = 0.00594(v/27)^2\left(10^{-5}h\right)^{10}\exp(-h/1000) + 2.7\times10^{-16}\exp(-h/1500) + A\exp(-h/100) \quad (17)$$

where v is the average wind speed, A is the typical constant of the surface refractive index of the atmosphere. The outer scale of turbulence as a function of altitude h can be expressed as (18), shown at the bottom of the page [29].

Assuming that $\delta = 0.1$ and the propagation distance of vertical is 20km, the relationship between pulse broadening ratio and initial pulse width under weak and strong turbulence are obtained and shown in Fig. 3.

Fig. 3(a) shows the relationship between pulse broadening ratio and initial pulse width under weak turbulence (the turbulence intensity is $C_n^2 = 10^{-15}\mathrm{m}^{-2/3}$). The pulse broadening ratio reduce drastically with the increasing of initial pulse width. When the initial pulse width is higher than 50*fs*, the downward trend of pulse broadening ratio slows down and gradually stability, and the pulse broadening ratio is close to 1. The pulse broadening effect of small zenith angle is weaker than large zenith angle. When the zenith angle become larger, the actual propagation distance of light become farther, and the influence of atmospheric turbulence become more serious under the same vertical propagation distance. Fig. 3(b) shows the pulse broadening under strong turbulence (the turbulence intensity is $C_n^2 = 10^{-13}\mathrm{m}^{-2/3}$). The variation trend of the curve corresponding to different zenith angle are roughly same as weak turbulence. However, when the initial pulse width is small (t_0<50*fs*), the pulse broadening caused by strong turbulence is much larger than weak turbulence. When t_0>100*fs*, the pulse broadening effect decreases gradually and tends to be stable.

In conclusion, the transmission of femtosecond laser is affected by turbulence seriously. But in actual PPM, the pulse width are sub nanosecond and nanosecond generally. According to Eq. (10), the influence of atmospheric turbulence on PPM optical communication rate can be ignored.

III. Detection Experiment

The scattering mechanism of particles with different sizes are not same, and different scattering processes are usually distinguished by the size parameter ($\alpha = 2\pi r/\lambda$, λ is the laser wavelength, r is the particle radius). The scattering process is Rayleigh scattering when the size parameter of scattering

$$L_0(h) = \begin{cases} \frac{4}{1+[(h-8500)/2500]^2}, & 2000 \le h \le 17000 \\ 0.307 - 0.0324\left(\frac{h}{1000} - 17\right) + 0.00167\left(\frac{h}{1000} - 17\right)^2 + 0.000476\left(\frac{h}{1000} - 17\right)^3 & h > 17000 \\ 3.21h^{-0.11}, & 1000 < h < 2000 \end{cases} \quad (18)$$

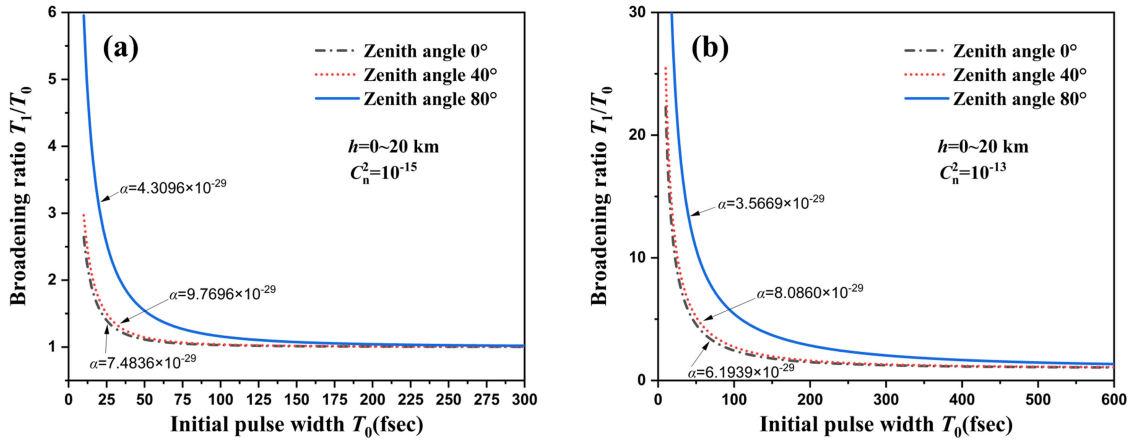

Fig. 3. (a) Relationship between pulse broadening ratio and initial pulse width under weak turbulence; (b) Relationship between pulse broadening ratio and initial pulse width under strong turbulence.

Fig. 4. The Aircraft Xinzhou 60 and detection equipment.

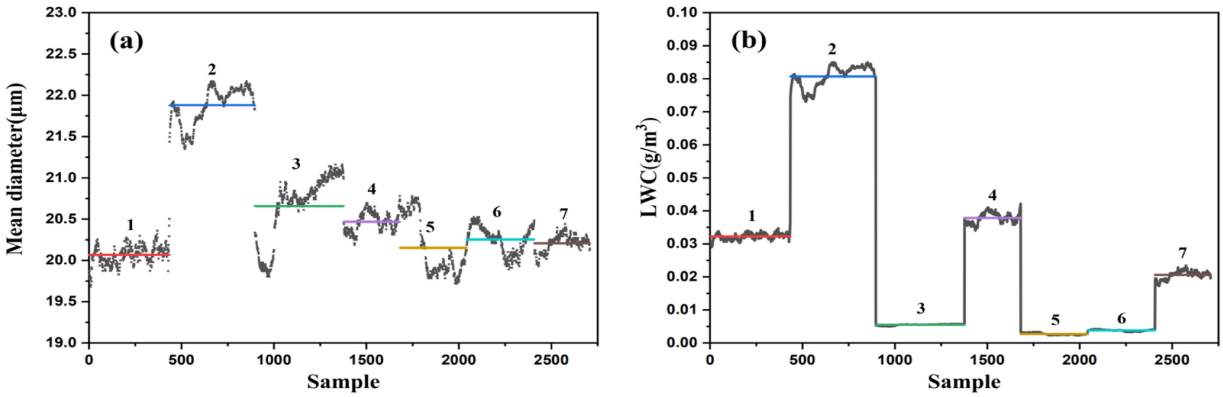

Fig. 5. Detection data of aircraft. (a) The average particle diameter of seven groups, (b) The atmospheric water content of seven groups.

TABLE I
THE ENVIRONMENT DATA OF CIRRUS

SAMPLE	1	2	3	4	5	6	7
LWC	0.03226	0.08071	0.005504	0.03787	0.002731	0.003813	0.02058
D	20.0661	21.8769	20.6602	20.4678	20.1521	20.2533	20.2070
Q_{ext}	2.0382	2.0207	2.0500	2.0486	2.0412	2.0442	2.0429

particles less than 0.1; The scattering process is Mie scattering when the size parameter of scattering particles larger than 0.1; When the size parameter is more than 50, the scattering process is geometrical optical scattering. Mie scattering is mainly considered when analyzing the multipath effect. Assuming that the communication wavelength is 1550nm, the cloud particles with the size range of 0.02∼12.3nm are mainly detected in this paper.

The detection equipments are the cloud particle detector on aircraft (Forward scattering cloud-droplet spectrum prober (FSSP-ER), Two-dimensional cloud particle spectrometer (2D-C) and Two-dimensional precipitation particle spectrometer (2D-P)), and the detection range of particle diameter is set as 1∼26μm.

The aircraft (Xinzhou 60) of Jilin Weather Modification Office carried out the detection mission among September and October 2020. The ground observation shows that the sky is clear and the cloud coverage area is less than 3/8. Cirrus predominate in the sky. The detector detected the target Cirrus for the first time when the flight altitude of the aircraft reaches 7300m. The detection equipments and aircraft are shown in Fig. 4.

The detection position is observed through the external monitor of the aircraft, and the detection time of the aircraft flying into and out the cirrus were recorded. The detection data with corresponding time are extracted, and the invalid data is eliminated. The average particle diameter and the atmospheric water content are shown in Fig. 5.

Table I shows seven groups of cirrus environment data obtained from multiple detection (Oct. 2020). Sample 1, sample 4 and sample 7 are feather cirrus, Sample 2 is deny cirrus, and sample 3, sample 5 and sample 6 are fake cirrus. These data of even groups will be used for simulation in this paper.

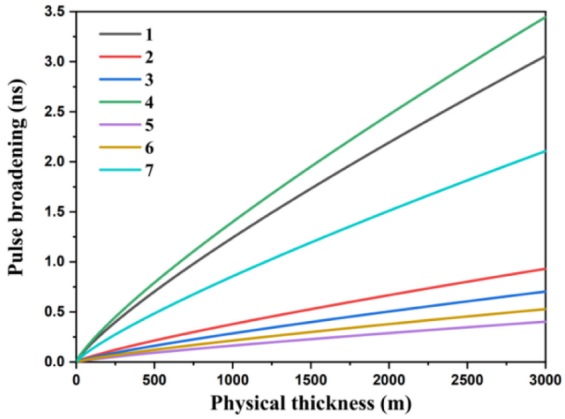

Fig. 6. Pulse broadening versus cloud physical thickness in different liquid water contents.

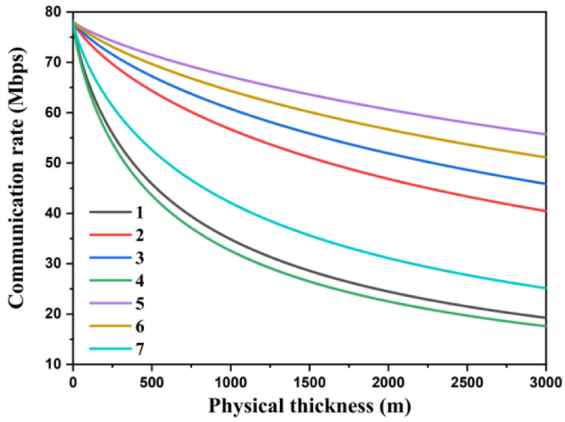

Fig. 7. Relationship between maximum communication rate and cloud thickness (32PPM, 1ns).

IV. RESULTS AND DISCUSSION

In this paper, we assume that the slot time is the same as the width of the broadened pulse all the time, and the power density function of the atmospheric channel is not taken into consideration. Fig. 6 shows the variation of laser pulse broadening with cloud physical thickness under different cloud parameters.

We can see from Fig. 6 that the cloud has a significant impact on pulse broadening. The broadened time is less than 3.5*ns* when the cloud physical thickness is 3000m. Therefore, the pulse broadening amplitude can be controlled within a allowable range even when the thickness reaches 3000m. According to Eq. (9), the broadening time is directly proportional to the atmospheric water content and inversely proportional to the particle size. The broadening time can not be judged completely by the statistical characteristics of cirrus clouds.

In order to illustrate the rate change of PPM optical communication system, the relationship between communication rate and cloud physical thickness with different cirrus clouds are shown in Fig. 7. It gives the relationship between laser communication rate and cloud physical thickness under 32-PPM modulation when the initial pulse width is 1*ns*. With the increase of cloud physical thickness, the laser communication rate decreases and finally remains stable. The influence of sample 4 is much stronger than sample 5 under the same PPM orders and initial pulse width.

Fig. 8 shows the relationship between the maximum communication rate and cloud thickness with different PPM orders (M). The laser communication rate at low PPM orders is higher than high PPM orders. The communication rate show great

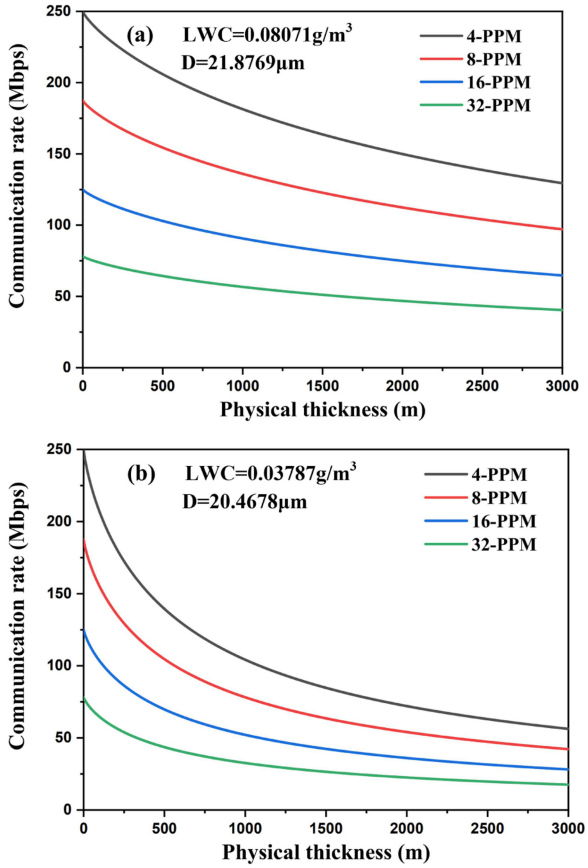

Fig. 8. Influence of communication rate by different PPM orders.(a) LWC = 0.08071g/m^3, D = 21.8769μm, (b)LWC = 0.03787g/m^3, D = 20.4678μm.

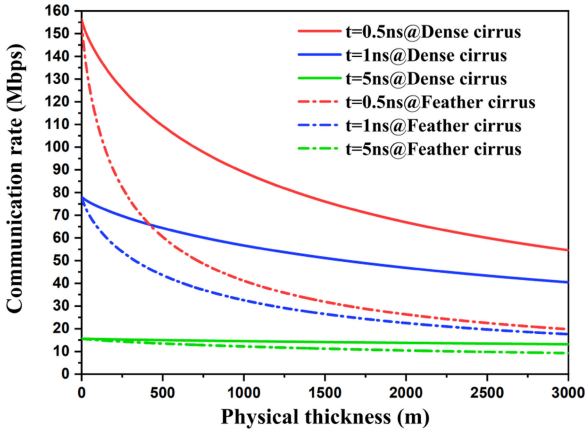

Fig. 9. Influence of communication rate by different initial pulse width (0.5ns, 1ns and 5ns).

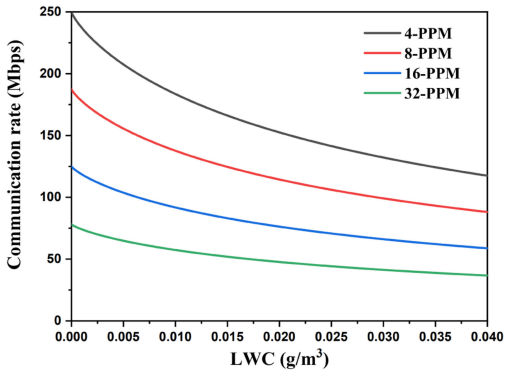

Fig. 10. Relationship between maximum communication rate and atmospheric water content under different PPM orders with 1ns initial pulse width.

affected by cirrus cloud with the decrease of modulation elements. Fig. 8(a) represents deny cirrus and Fig. 8(b) represents feather cirrus. The feather cirrus have greater impact on the communication rate through comparison. For example, $R_{\text{c-4PPM}}$ = 149.9Mbps, $R_{\text{c-16PPM}}$ = 112.4Mbps, $R_{\text{c-8PPM}}$ = 74.9Mbps, $R_{\text{c-32PPM}}$ = 46.8Mbps (@T = 2000m, dense cirrus); $R_{\text{c-4PPM}}$ = 72Mbps, $R_{\text{c-16PPM}}$ = 54Mbps, $R_{\text{c-8PPM}}$ = 36Mbps, $R_{\text{c-32PPM}}$ = 22.5Mbps (@T = 2000m, feather cirrus), feather cirrus have greater impact on laser communication than dense cirrus.

The effects of different initial pulse width are analyzed under the conditions of dense cirrus and feather cirrus. With the increase of cirrus physical thickness, the laser communication rate decreases and finally remains stable. Fig. 9 shows that the rate under dense cirrus is higher than that under feather cirrus, and the difference is obvious. Besides, the rates falls down sharply when the initial pulse width is 0.5*ns*. It means that the initial pulse width becomes much narrower, the performance of the laser communication system degrades more severely.

According to Eq. (9), the scattering optical thickness is directly proportional to the extinction efficiency factor and inversely proportional to the average size of cloud particles. The accurate detection of cloud particles is difficult. The detection accuracy of sounding balloon is low. Aircraft cloud detection needs to be supervised by air traffic control and the cost is very high.

In order to predict the impact of cirrus clouds on communication rate, finally realize stable and high-speed laser communication, the impact of real-time cirrus clouds on PPM communication rate can be retrieved through ground atmospheric water content detection. The relationship between the maximum communication rate and atmospheric water content are analyzed through the statistical average data measured by aircraft. The result is shown in Fig. 10. According to the results of local meteorological statistics, the thickness of cirrus clouds in Changchun is distributed among 0.3∼1.5km, and the average thickness is about 0.73km. The average particle size in this paper is set as 20.5262 through the aircraft test results (detection results of Xinzhou 60 in Jilin Weather Modification Office). And the value of water content is 0.04-0.003 according to the the aircraft test results.

V. Conclusion

Pulse position modulation has a promising prospect for improving the data transmission rate of deep space optical communication system, but the optical channel will exert attenuation on the communication rate. In this paper, the data transmission rate attenuation caused by pulse broadening are investigated. The general formulas of the rate attenuation caused by cloud scattering was presented. Combined with the actual application

site, the pattern and physical characteristics of cloud are detected by aircraft and then analyzed. The measured data of aircraft are used for numerical simulation. Numerical simulation results indicate that the rate attenuation increase strongly initially with the increase of cloud physical thickness and aerosol optical thickness, and then shows a tendency toward stabilization. Both the lower modulation orders and the smaller initial pulse widths can improve the data rate greatly when the thickness are small. Because the aircraft detection process is difficult, statistical values of particle size are used when analyzing the impact of cirrus clouds in Changchun. Then the real-time water vapor content are combined with statistical values of particle size to analyze the impact of cirrus clouds on ppm communication rate. This work can provide reference for the parameters selection of DSOC system, and one can adjust the optimum communication rate according to the results of atmosphere channel monitoring.

REFERENCES

[1] H. L. Jiang and S. F. Tong, "*The Technologies and Systems of Space Laser Communication*," Beijing, China: National Defence Industry Press, 2010, pp. 5–10.

[2] J. Ma, K. Li, L. Tan, S. Yu, and Y. Cao, "Performance analysis of satellite-to-ground downlink optical communications with spatial diversity over gamma-gamma atmospheric turbulence," *Appl. Opt.*, vol. 54, no. 25, pp. 7575–7585, 2015.

[3] J. Ma, G. Lu, S. Yu, L. Tan, and F. Li, "Fiber coupling efficiency for satellite and space to ground downlinks with pointing errors," *Optik - Int. J. for Light Electron Opt.*, vol. 202, 2019, Art. no. 163558.

[4] D. M. Boroson *et al.*, "Overview and results of the lunar laser communication demonstration," *SPIE*, vol. 8971, pp. 1–11, 2014.

[5] H. Ivanov, E. Leitgeb, P. Pezzei, and G. Freiberger, "Experimental characterization of SNSPD receiver technology for deep space FSO under laboratory testbed conditions," *Optik - Int. J. for Light Electron Opt.*, vol. 195, 2019, Art. no. 163101.

[6] D. M. Boroson and B. S. Robinson, "The lunar laser communication demonstration: NASA's first step toward very high data rate support of science and exploration missions," *Space Sci. Rev.*, vol. 185, pp. 115–128, 2014.

[7] B. Mohamed, F. M. Abbou, M. Serhani, F. Chaatit, and A. Boutoulout, "Temporal pulse broadening due to dispersion and weak turbulence in fso communications," *Optik - Int. J. for Light Electron Opt.*, vol. 200, Jan. 2020, Art. no. 163327.

[8] A. Biswas *et al.*, "LLCD operations using the optical communications telescope laboratory (OCTL)," *Proc. SPIE*, vol. 8971, pp. 450–453, 2014.

[9] N. Kumar, "2.50 Gbit/s optical wireless communication system using PPM modulation schemes in HAP-to-satellite links," *Optik - Int. J. for Light Electron Opt.*, vol. 125, no. 14, pp. 3401–3404, 2014.

[10] A. Biswas, V. Vilnrotter, W. Farr, D. Fort, and E. Sigman, "Pulse position modulated (PPM) ground receiver design for optical communications from deep space," *Proc. SPIE*, vol. 4635, pp. 224–235, 2002.

[11] M. D. Rayman and D. L. Robinson, "Modulation techniques for deep-space pulse-position modulation (PPM) optical communication," *Proc. SPIE*, vol. 885, pp. 32–35, 1998.

[12] W. Gappmair and S. S. Muhammad, "Error performance of terrestrial FSO links modelled as PPM/Poisson channels in turbulent atmosphere," *Electron. Lett.*, vol. 43, pp. 63–64, 2007.

[13] W. Gappmair and S. S. Muhammad, "Error performance of PPM/Poisson channels in turbulent atmosphere with gamma-gamma distribution," *Electron. Lett.*, vol. 43, pp. 880–882, 2007.

[14] N. D. Chatzidiamantis, H. G. Sandalidis, G. K. Karagiannidis, and M. Matthaiou, "A simple statistical model for turbulence-induced fading in free-space optical systems," in *Proc. IEEE Int. Conf. Commun.*, Cape town, South Africa, 2010, pp. 1–5.

[15] N. C. Beaulieu and L. Cao, "Robust and accurate BER computation for M-ary orthogonal signaling on a discrete memoryless channel," in *Proc. Conf. Elect. Comput. Eng.*, 2005, pp. 1177–1179.

[16] J. Hamkins, "Accurate computation of the performance of M-ary orthogonal signaling on a discrete memoryless channel," *IEEE Trans. Commun.*, vol. 52, no. 11, pp. 1844–1845, Nov. 2004.

[17] B. Enzo, B. Mauro, P. Cristian, and C. Nicola, "Optimal MIMO UWB-IR transceiver for Nakagami-fading and poisson-arrivals," *J. Commun. Netw.*, vol. 3, no. 1, pp. 27–40, 2008.

[18] M. Biagi and A. M. Vegni, "Enabling high data rate VLC via MIMO-LEDs PPM," in *Proc. IEEE Globecom Workshops*, 2013, pp. 1058–1063.

[19] S. Dolinar, D. Divsalar, and J. Hamkins, "Capacity of pulse-position modulation (PPM) on Gaussian and Webb channels," *Interplanetary Netw. Prog. Rep.*, vol. 142, pp. 314–317, 2000.

[20] B. Moision and J. Hamkins, "Deep-space optical communications downlink budget: Modulation and coding," *Interplanetary Netw. Prog. Rep.*, vol. 154, pp. 17674–17680, 2003.

[21] R. Z. H. Rao, *Modern Atmospheric Optics*. Beijing, China: Science Press, 2012, pp. 220–235.

[22] E. A. Bucher, R. M. Lerner, C. W. Niessen, "Some experiments on the propagation of light pulses through clouds," *Appl. Opt.*, vol. 58, pp. 1564–1567, 1970.

[23] H. Hemmati, *Deep Space Optical Communication*. New York, NY, USA: Wiley, 2006.

[24] L. Y. Xing, H. T. Zhang, M. Zhang, and L. Fu. "Analysis of surface meteorological observation (manual) data of changchun national reference climate station from 1956 to 2018," *Technol. Econ. Guide*, vol. 686, no. 24, pp. 97–98, 2019.

[25] D. Van and V. Twersky, "Light scattering by small particles," *Phys. Today*, vol. 10, no. 12, pp. 28–30, 1957.

[26] M. D. King *et al.*, "Remote sensing of liquid water and ice cloud optical thickness and effective radius in the arctic: Application of airborne multispectral MAS data," *J. Atmospheric Ocean. Technol.*, vol. 21, no. 6, 2004, Art. no. 857.

[27] Y. Ping, K. N. Liou, K. Wyser, and D. Mitchell, "Parameterization of the scattering and absorption properties of individual ice crystals," *J. Geophysical Res.: Atmospheres*, vol. 105, no. D4, pp. 4699–4718, 2000.

[28] D. E. Tjin tham sjin and L. C. Andrews, "Temporal broadeningand scintillations of ultrashort optical pulses," *Waves in Random Media*, vol. 9, no. 3, pp. 307–325, 1999.

[29] C. E. Coulman, J. Vernin, Y. Coqueugniot, and J. L. Caccia, "Outer scale of turbulence appropriate to modeling refractive-index structure profiles," *Appl. Opt.*, vol. 27, no. 1, pp. 155–160, 1988.